American Mineralogist, Volume 89, pages 640–646, 2004

Synthesis and crystal-chemistry of $Na(NaMg)Mg_5Si_8O_{22}(OH)_2$, a $P2_1/m$ amphibole

GIANLUCA IEZZI,[1,2,†] GIANCARLO DELLA VENTURA,[2,*] ROBERTA OBERTI,[3] FERNANDO CÁMARA,[3] AND FRANÇOIS HOLTZ[4]

[1]Bayerisches Geoinstitut, Universität Bayreuth, D-95440 Bayreuth, Germany
[2]Dipartimento di Scienze Geologiche, Università di Roma Tre, Largo S. Leonardo Murialdo 1, I-00146 Roma, Italy
[3]CNR-Istituto di Geoscienze e Georisorse, sezione di Pavia, via Ferrata 1, I-27100 Pavia, Italy
[4]Institut für Mineralogie, Universität Hannover, Welfengarten 1, D-30167, Germany

ABSTRACT

In the present work, we characterize the amphibole $Na(NaMg)Mg_5Si_8O_{22}(OH)_2$ synthesized at 0.4 GPa and 750, 800, and 850 °C, and 0.5 GPa, 900 °C. Experiments at 800 and 900 °C yielded crystals suitable for single-crystal data collection. Structure refinement shows that synthetic $Na(NaMg)Mg_5Si_8O_{22}(OH)_2$ has $P2_1/m$ symmetry at room T. The two non-equivalent tetrahedral double-chains differ in their degree of stretching and kinking. The infrared spectrum of synthetic $Na(NaMg)Mg_5Si_8O_{22}(OH)_2$ has two well-defined absorption bands at 3742 and 3715 cm^{-1} which can be assigned to O-H bands associated with the two independent anion sites (O3A and O3B) in the structure. The higher frequency band is assigned to the shorter O3B-H2 bond, and the lower frequency band is assigned to the longer O3A-H1 bond. The broader shape of the 3743 cm^{-1} band is consistent with a stronger interaction of the H2 atom with ^{A}Na, which is confirmed by structure refinement. Increasing T of synthesis causes a progressive departure from the ideal stoichiometry via the $^{A}\square_1{}^{B}Mg_1{}^{A}Na_{-1}{}^{B}Na_{-1}$ substitution, as confirmed by EMPA, structure refinement, and FTIR spectroscopy.

INTRODUCTION

$Na(NaMg)Mg_5Si_8O_{22}(OH)_2$ is an interesting amphibole composition not found in nature, but repeatedly investigated in experimental work (Gibbs et al. 1962; Gier et al. 1964; Witte et al. 1969; Maresch and Langer 1976; Raudsepp et al. 1991; Liu et al. 1996). This amphibole is one of the structural modules of triple-chain silicates, in particular of the sodium variety of clinojimthompsonite, $Na_4Mg_8Si_{12}O_{32}(OH)_4$; therefore, investigation of its stability is also relevant to the study of biopyriboles. $Na(NaMg)Mg_5Si_8O_{22}(OH)_2$ can be easily synthesized at low P with very high yields of extremely acicular and well-formed crystals, generally less than 1 or 2 μm in width (Gibbs et al. 1962; Raudsepp et al. 1991). Despite the simple chemical composition and ease of synthesis, details of the crystal structure are still obscure, and two different monoclinic space groups, $C2/m$ (Witte et al. 1969) and $P2_1/m$ (Liu et al. 1996), have been suggested from X-ray powder diffraction data. Experimental work in the Na_2O-MgO-SiO_2-H_2O system also showed the existence of a stable amphibole composition with three protons per formula unit, i.e., $NaNa_2Mg_5Si_8O_{21}(OH)_3$, which is related to $Na(NaMg)Mg_5Si_8O_{22}(OH)_2$ by the $Na_1H_1Mg_{-1}$ exchange. The former amphibole is triclinic at room T, and undergoes a complex triclinic-to-monoclinic $C\bar{1} \rightarrow C2/m$ phase transition in the T range 100-160 °C (Maresch et al. 1991; Liu et al. 1996).

$P2_1/m$ symmetry in amphiboles is usually confined to the Mg-rich side of the cummingtonite solid-solution, and converts to $C2/m$ symmetry typical of rock-forming amphiboles as a function of increasing X_{Fe} and/or T. Oberti et al. (2000) revisited a sample synthesized by W. Maresch and co-workers during a systematic study of the LiO_2-Na_2O-MgO-SiO_2-H_2O system (cf. Maresch and Langer 1976 for details). Using a combination of electron- and ion-microprobe analysis (EMPA, SIMS), single-crystal X-ray refinement (SREF) diffraction, and Fourier-Transform Infrared Spectroscopy (FTIR), Oberti et al. (2000) showed that this amphibole has $P2_1/m$ symmetry, and the structural formula $Na_{0.95}(Mg_{0.97}Li_{0.27}H_{0.12}Na_{0.64})Mg_5Si_8O_{22}(OH)_2$, with a small but significant OH excess ordered at the B-group sites. While providing the first direct evidence of a primitive space-group in an A-site occupied amphibole, these authors could not, however, explain the structural reasons for its occurrence.

We report in this paper on the compositional variation, crystal-structure, and crystal-chemistry, as determined using a combination of EMPA, SREF, and FTIR analysis, of a series of samples of nominal composition $Na(NaMg)Mg_5Si_8O_{22}(OH)_2$, synthesized under different T and P conditions.

EXPERIMENTAL METHODS

Two sets of samples were synthesized, one in an F-free and the other in an F-rich system. Table 1 reports experimental conditions and sample labels. Starting products were prepared both as silicate gels for the OH-bearing composition using the method of Hamilton and Henderson (1968), and as mixtures of NaF, MgO, and SiO_2 for F-bearing compositions. Sample 403 was synthesized using a 4 M solution of NaBr instead of pure water to improve the crystal size (Zimmerman et al. 1996). Hydrothermal synthesis was done using an internally heated pressure vessel at the University of Hannover with Ar as the pressure medium. Pressure was continuously monitored by a transducer (accuracy of ±5 MPa), and the temperature was controlled by two type-K thermocouples placed around the hot-spot

* E-mail: dellaven@uniroma3.it
† Presently at: Dipartimento di Scienze della Terra, Università "G. D'Annunzio", I-66013 Chieti Scalo, Italy

(Wilke et al. 2002 and references therein). Two additional thermocouples placed near the capsule showed that the temperature gradient along the tube was <10 °C. Quenching was done by switching off the power supply; the estimated quenching rate was 200–300 °C/min.

Step-scan X-ray powder-patterns were collected with a Scintag X1 diffractometer operated in the vertical θ-θ configuration with Ni-filtered Cu$K\alpha$ radiation and a Si(Li) solid-state detector. Unit-cell dimensions were refined by whole-powder-pattern refinement (Rietveld method) using DBW3.2 (Wiles and Young 1981).

Single crystals suitable for X-ray analysis were hand-picked from the products of experiments 334 and 403. Data collections was done with a Bruker-AXS SMART-Apex single-crystal diffractometer using graphite-monochromatized Mo$K\alpha$ X-radiation at 55 kV and 30 mA; the crystal-to-detector distance was 4.0 cm. Three-dimensional data were integrated and corrected for Lorentz, polarization, and background effects using the SAINT+ software version 6.02 (Bruker AXS). Unit-cell dimensions were calculated from least-squares refinement of the positions of all the collected reflections. For crystal 334, with a size of 220 × 90 × 20 μm, a frame width of 0.2° in ω was used to collect 840 frames per batch for four batches at different ϕ values (0°, 90°, 180°, 270°) with 30 s counting time per image. For crystal 403, with a size of 150 × 15 × 15 μm, a frame width of 0.2° in ω was used to collect 750 frames per batch for two batches at different ϕ values (0°, 70°) with 120 s counting time per image. Raw intensity data were corrected for absorption using the SADABS v. 2.03 program (Sheldrick 1996).

For crystal 334, reflections with $I > 3\sigma_I$ were considered as observed during unweighted full-matrix least-squares refinement on F using a program specifically written at the CNR-IGG-PV to deal with complex solid-solutions. The occupancies of the M1, M2, and M3 sites were first refined (maximum deviation from Mg occupancy <1%) and then fixed to Mg = 1 in the final cycles. For crystal 403, the very low intensity of most of the reflections required a weighted refinement on all the reflections. The weighting scheme used is the same as in the SHELXTL program (Sheldrick 1997). To minimize the number of variables, the occupancies of the O, T, M1-3 sites and the atomic-displacement factors (adp) were kept fixed to the values obtained for crystal 334. In this way, a reasonable estimate of the A and M4 site-occupancies was obtained, whereas the refined coordinates are affected by the constraints given to the adps, and are not reported in the tables. Scattering curves for fully ionized chemical species were used at those sites where chemical substitutions occur; neutral vs. ionized scattering curves were used at the T and anion sites. Selected crystal data and refinement information are given in Table 2. Atom positions and displacement parameters are given in Table 3, and selected interatomic distances and angles are given in Table 4. Table 5[1] lists observed and calculated structure factors. A sketch of the structure and site nomenclature for sample 334 n. 2 is given in Figure 1.

FTIR spectra in the OH-stretching region (4000–3000 cm^{-1}) were collected at room temperature with a Nicolet 760 spectrophotometer equipped with a DTGS detector and a KBr beamsplitter. The nominal resolution was 2 cm^{-1}; spectra are the average of 64 scans. Samples were prepared as KBr pellets; digitized spectra were fitted by interactive optimization followed by least-squares refinement. The background was modeled as linear, and all peaks were modeled as symmetric Gaussian functions (Strens 1974). Details of the fitting procedure can be found in Della Ventura et al. (1996).

Samples for electron-microprobe analysis were prepared by embedding a few milligrams of amphibole powder in epoxy resin. After careful polishing, a few grains with a size acceptable for analysis were found in all the samples, but most crystallites were very small (average dimension 2 × 40 μm). EMP analysis was done at the Bayerisches Geoinstitut with a fully automated CAMECA SX-50 microprobe operating in WDS mode with a 15 kV excitation voltage, a 10 nA beam current, a 10 s counting time on peak and 5 s counting time on background. A short counting time was used to prevent sodium volatilization from the sample. Minerals were used as standards: Na and Si were quantified with reference to albite (TAP), Mg to enstatite (TAP), and F to apatite (TAP). Data reduction used the PAP method (Pouchou and Pichoir 1984, 1985).

[1] For a copy of Table 5, Document AM-04-062, contact the Business Office of the Mineralogical Society of America (see inside cover of a recent issue for price information). Deposit items may also be available on the American Mineralogist web site at http://www.minsocam.org.

TABLE 1. Sample labels and experimental conditions

F-free experiments	F-doped experiments	T (°C)	P (GPa)	Duration (days)
371	372	750	0.4	10
403	--	800	0.4	7
351	352	850	0.4	7
333	334	900	0.5	6

TABLE 2. Selected crystal and refinement data

	334 n.2	403 n.2
a (Å)	9.689(1)	9.735(3)
b (Å)	17.938(2)	17.942(4)
c (Å)	5.268(5)	5.274(1)
β (°)	102.50(3)	102.33(1)
V (Å³)	893.9	899.9
Space group	$P2_1/m$	$P2_1/m$
θ range (°)	2–35	2–30
threshold cut	3σ (I)	0σ (I)
no. all	4036	2717
no. obs	2468	2717
R sym × 100	4.0	17.5
R obs × 100	4.1	[6.5 for 3σ (I)]
R all × 100	7.7	17.8
ss* at A	8.1	10.2
ss at B	23.4	22.4

* ss = refined site-scattering values at the group sites (electrons per formula unit).

RESULTS

Experimental products: EMP and X-ray powder data

Synthetic products were characterized by powder XRD, and by optical and electron microscopy (SEM-EDAX). Very high amphibole yields (>90%) were obtained at higher T conditions. Additional phases were detected by SEM microscopy and powder diffraction: quartz plus rare enstatite, the amount of which increased in the lower T experiments (up to 15% for sample 372, from Rietveld analysis of the powder spectrum). Amphibole crystals (Fig. 2) are acicular and prismatic in the **c** direction; their size rarely exceeds 100 × 5 μm. Generally, grain size increases slightly with the T of synthesis, and is larger in the F-doped samples. EMP analysis of all experimental products (Table 6) yielded nil or very small F contents (~0.04 wt%), indicating that F is not incorporated into the amphibole structure under the hydrous experimental conditions used. The experimental products obtained at the same T in the different charges were considered identical, and the choice of samples in the subsequent SREF analysis was based only on crystal size. Table 6 shows a progressive departure of the amphibole from the nominal composition with increasing T. The active exchange vector is $^{A}\square_{1}{}^{B}Mg_{1}{}^{A}Na_{-1}{}^{B}Na_{-1}$. This feature is confirmed by both SREF

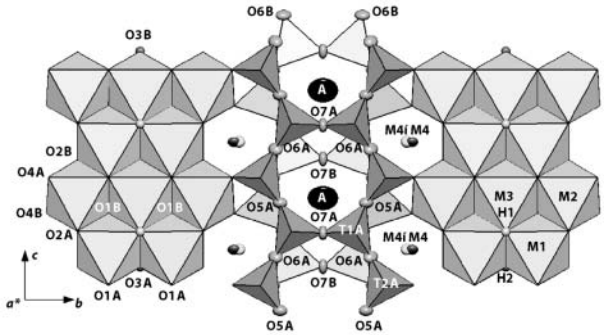

FIGURE 1. Structure and site nomenclature for nominal $Na(NaMg)Mg_5Si_8O_{22}(OH)_2$. Projection onto (100). Ellipsoids are drawn at 95% probability. Images made using XtalDraw (Downs and Hall-Wallace 2003).

TABLE 3. Atomic coordinates, isotropic equivalent (Å^2), and anisotropic atom-displacement factors (×10^4) for crystal 334 n. 2

Site	*x*	*y*	*z*	B_{eq}	β_{11}	β_{22}	β_{33}	β_{12}	β_{13}	β_{23}
O1A	–0.1369(3)	0.3368(2)	0.1973(5)	0.58	17(2)	3(1)	69(8)	2(1)	11(3)	–2(2)
O1B	0.3629(3)	0.8366(1)	0.2255(5)	0.57	21(2)	4(1)	47(8)	–3(1)	10(3)	1(2)
O2A	–0.1302(3)	0.4217(2)	0.7018(5)	0.77	19(2)	8(1)	61(8)	0(1)	10(3)	–3(2)
O2B	0.3734(3)	0.9219(1)	0.7355(5)	0.72	19(2)	5(1)	85(8)	–1(1)	14(3)	–2(2)
O3A	–0.1394(4)	1/4	0.6943(7)	0.68	21(4)	5(1)	64(11)	0	8(5)	0
O3B	0.3577(4)	3/4	0.7221(8)	0.72	19(4)	4(1)	89(12)	0	10(5)	0
O4A	0.1199(4)	0.4993(2)	0.7959(6)	1.16	46(3)	5(1)	99(10)	–7(1)	-5(4)	–2(2)
O4B	0.6258(4)	0.9938(2)	0.7658(7)	1.80	60(4)	8(1)	159(12)	–19(1)	-34(5)	21(2)
O5A	0.0969(3)	0.3674(2)	0.0237(5)	1.00	25(3)	9(1)	92(9)	2(1)	15(3)	12(2)
O5B	0.6002(3)	0.8854(2)	0.0969(5)	0.97	22(3)	10(1)	85(9)	0(1)	11(4)	13(2)
O6A	0.0994(3)	0.3800(2)	0.5277(5)	1.07	25(3)	10(1)	92(9)	4(1)	6(4)	–18(2)
O6B	0.5934(3)	0.8578(2)	0.5964(5)	1.07	22(2)	11(1)	87(9)	1(1)	6(3)	–11(2)
O7A	0.0921(4)	1/4	0.2998(8)	0.94	17(3)	5(1)	156(14)	0	16(5)	0
O7B	0.5905(4)	3/4	0.2613(8)	0.83	23(4)	2(1)	139(13)	0	21(5)	0
T1A	0.0324(1)	0.3355(1)	0.2619(2)	0.54	17(1)	3(1)	52(3)	0(1)	7(1)	0(1)
T1B	0.5321(1)	0.8346(1)	0.2949(2)	0.52	17(1)	4(1)	47(3)	0(1)	9(1)	1(1)
T2A	0.0408(1)	0.4214(1)	0.7677(2)	0.53	17(1)	3(1)	53(3)	–1(1)	7(1)	0(1)
T2B	0.5439(1)	0.9195(1)	0.7989(2)	0.67	21(1)	5(1)	56(3)	–3(1)	6(1)	1(1)
M1	–0.2499(2)	0.3382(1)	0.4850(3)	0.65	22(1)	4(1)	64(4)	0(1)	11(2)	–1(1)
M2	–0.2503(2)	0.4295(1)	0.9842(3)	0.66	21(1)	4(1)	70(4)	0(1)	13(2)	2(1)
M3	–0.2494(2)	1/4	0.9859(4)	0.62	23(1)	4(1)	53(5)	0	11(2)	0
M4	–0.2461(3)	0.5054(1)	0.4840(5)	0.84	26(2)	6(1)	91(9)	1(1)	28(3)	5(2)
A	0.2654(5)	1/4	0.0462(11)	3.56	63(5)	38(2)	413(24)	0	130(9)	0
M4'	–0.2592(4)	0.5202(2)	0.4772(7)	1.17						
H1	–0.053(10)	1/4	0.751(19)	3.28						
H2	0.566(9)	1/4	0.241(17)	1.87						

FIGURE 2. SEM-SE image of sample 403. The scale bar is 10 μm.

TABLE 4. Selected interatomic distances (Å) and angles (°)

		334 n. 2		334 n.2
T1A-O1A		1.602(3)	T1B-O1B	1.601(3)
T1A-O5A		1.622(3)	T1B-O5B	1.629(3)
T1A-O6A		1.620(2)	T1B-O6B	1.626(3)
T1A-O7A		1.636(2)	T1B-O7B	1.642(2)
<T1A-O>		1.620	<T1B-O>	1.624
T2A-O2A		1.618(3)	T2B-O2B	1.614(3)
T2A-O4A		1.584(3)	T2B-O4B	1.579(3)
T2A-O5A		1.653(3)	T2B-O5B	1.663(3)
T2A-O6A		1.669(3)	T2B-O6B	1.677(3)
<T2A-O>		1.631	<T2B-O>	1.633
M1-O1A		2.053(3)	M2-O1A	2.167(3)
M1-O1B		2.061(3)	M2-O1B	2.159(3)
M1-O2A		2.078(3)	M2-O2A	2.082(3)
M1-O2B		2.104(3)	M2-O2B	2.094(3)
M1-O3A		2.087(3)	M2-O4A	1.985(3)
M1-O3B		2.072(3)	M2-O4B	2.016(3)
<M1-O>		2.076	<M2-O>	2.084
M3-O1A	×2	2.080(3)	$<^{[6]}$A-O>	2.616
M3-O1B	×2	2.082(3)	O3A-H1	0.824(4)
M3-O3A		2.050(4)	O3B-H2	0.723(4)
M3-O3B		2.041(4)	O5A-O6A-O5A	189.8(2)
<M3-O>		2.069	O5B-O6B-O5B	158.6(2)
M4-O2A		2.069(3)	M4'-O2A	2.334(3)
M4-O2B		2.118(3)	M4'-O2B	2.249(3)
M4-O4A		2.111(3)	M4'-O4A	2.203(3)
M4-O4B		2.131(4)	M4'-O4B	2.086(4)
M4-O6A		2.508(3)	M4'-O6A	2.371(3)
M4-O5B		2.983(3)	M4'-O5B	2.749(3)
M4-O6B		3.030(3)	M4'-O6B	2.758(3)
$<^{[5]}$M4-O>		2.188	$<^{[5]}$M4'-O>	2.249

and FTIR analyses, as discussed below. It is worth mentioning here that a ^{B}Mg-enrichment at high-*T* also occurs in tremolite (e.g., Jenkins 1987), where deviation from stoichiometry following the $^{B}Mg^{B}Ca_{-1}$ vector leads to thermal stabilization of the amphibole primarily due to entropic reasons. In tremolite, the configurational entropy terms maximizes at the $tr_{90}cum_{10}$ composition (cum = cummingtonite) (Jenkins 1987). This behavior may suggest that a similar entropic stabilization for increasing Mg at the M4 site is a significant factor in the system investigated here as well.

Powder X-ray diffraction patterns for all samples were indexed in $P2_1/m$; the refined unit-cell parameters and volumes are given in Table 7 and Figure 3. As expected from the observed crystal-chemical variations, the most sensitive parameters are the *a* dimension (the values of which mostly depends on the A-site occupancy) and the β angle (the value of which strongly depends on the site population, or more accurately on the aggregate ionic radius and charge at the B-sites). The *b* and *c* dimensions depend mainly on the octahedral and tetrahedral site populations, respectively, therefore they are virtually constant in this work. Changes in the unit-cell parameters along an amphibole solid solution are expected to be linear; on the contrary, the trends of the observed unit-cell parameters vs. the A-site population are significantly non-linear (Fig. 3). It should be noted that all these samples undergo a displacive second-order $P2_1/m \rightarrow C2/m$ transition at varying but rather low temperatures. A T_c of 257 ± 3 °C was obtained for crystal 334 n. 2 by Cámara et al. (2003), and evidence was found that it should decrease approaching the ideal $Na(NaMg)Mg_5Si_8O_{22}(OH)_2$ composition. This transition implies

TABLE 6. EMP analyses and calculated unit-formulae (24 O) for the synthetic amphiboles of this work. The estimated standard deviations of the point analyses are in parentheses; the number of reliable analyses depends on crystal size.

Sample	334	333	351	352	403	371	372
T (°C)	900	900	850	850	800	750	750
points	9	1	16	14	4	2	7
SiO_2	60.15 (24)	60.22	60.21(35)	60.33 (28)	59.67 (9)	59.71 (13)	60.15 (22)
MgO	31.24 (28)	31.16	30.62(32)	30.69 (27)	30.02(14)	30.09 (7)	30.17 (12)
Na_2O	6.34 (16)	6.44	7.23(12)	7.16 (16)	7.63 (8)	7.80 (19)	7.76 (9)
Total	97.73 (46)	97.82	98.06(59)	98.18 (49)	97.32(10)	97.60 (38)	98.08 (39)
Si	8.00 (2)	8.00	8.00 (2)	8.00 (1)	8.00 (1)	7.99 (1)	8.01 (1)
Mg oct	5.00	5.00	5.00	5.00	5.00	5.00	5.00
Mg M4	1.19 (3)	1.17	1.06 (4)	1.07 (3)	1.00 (3)	1.00 (1)	0.99 (1)
Na M4	0.81 (3)	0.83	0.94 (4)	0.93 (3)	1.00 (3)	1.00 (1)	1.01 (1)
Na A	0.82 (4)	0.83	0.93 (4)	0.91 (3)	0.98 (1)	1.03 (4)	0.99 (1)
OH	2.00	2.00	2.00	2.00	2.00	2.00	2.00
Σ *cations*	15.82 (4)	15.83	15.93	15.91	15.98	16.02	16.00
ss C*	60.00	60.00	60.00	60.00	60.00	60.00	60.00
ss B	23.19 (3)	23.17	23.06 (4)	23.07 (3)	23.00 (3)	23.00 (1)	22.99 (1)
ss A	9.06 (46)	9.13	10.21(49)	10.02 (37)	10.83(15)	11.32 (40)	10.89 (14)
ss tot	92.25 (47)	92.30	93.28(53)	93.09 (37)	93.84(16)	94.32 (16)	93.88 (14)

* ss = calculated site scattering at the different groups of sites.

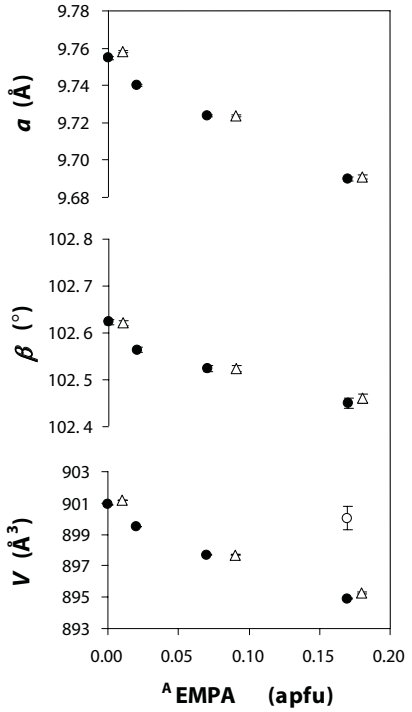

FIGURE 3. Unit-cell parameters measured for the samples of this work plotted as a function of the A-site vacancy estimated by EMPA (full circles = F-free syntheses; triangles = F-doped syntheses; errors within the size of the symbol). The open circle represents the unit-cell volume extrapolated for a hypothetical room-*T C*2/*m* structure from the high-*T* data of Cámara et al. (2003).

structural relaxation in the $P2_1/m$ space group, which is most evident for the neatly decreasing *b* and *c* dimensions and thus for the unit-cell volume; the much higher value of *V* extrapolated for an hypothetical room-*T C*2/*m* structure from the high-*T* data of Cámara et al. (2003) is also shown in Figure 3. Therefore, the observed non-linearity is coherent with the presence of macroscopic spontaneous strain related to the phase transition, the amount of which is also a function of composition.

TABLE 7. Lattice parameters refined from powder diffraction data for the samples of this work.

	a (Å)	*b* (Å)	*c* (Å)	β (°)	*V* (Å³)
333	9.6900(10)	17.935(2)	5.2730(10)	102.450(10)	894.90(5)
351	9.7238(6)	17.938(1)	5.2721(6)	102.524(6)	897.70(2)
403	9.7401(8)	17.940(1)	5.2739(6)	102.564(6)	899.50(2)
371	9.7548(8)	17.945(1)	5.2740(6)	102.623(6)	900.90(2)
334	9.6910(10)	17.940(3)	5.2730(10)	102.460(10)	895.30(6)
352	9.7238(6)	17.938(1)	5.2721(6)	102.524(6)	897.70(2)
372	9.7580(6)	17.948(1)	5.2732(5)	102.621(5)	901.20(1)

The F content of $Na(NaMg)Mg_5Si_8O_{22}(OH,F)_2$

Robert et al. (2000) and Della Ventura et al. (2001) showed that the OH-F solid-solution in amphiboles is strongly controlled by the local bond-valence arrangement around the O3 atoms, i.e., by the degree of local interaction of the OH group with the NNN O atoms. Accordingly, the OH groups involved in weak hydrogen-bonding, and characterized by higher-frequency of vibration in the IR spectra, are easily exchanged with F, whereas those involved in strong hydrogen-bonding, typically characterized by a low principal-stretching frequency in IR spectra, are not easily exchanged. This behavior was observed in pargasite (Robert et al. 2000) and in pargasite-richterite solid-solutions (Della Ventura et al. 2001), where OH-F exchange strongly depends on the ordering of octahedral cations. For example, the incorporation of OH in pargasite is greatly favored in water-bearing systems and allows ^{VI}Al disorder between the M2 and M3 sites, whereas $NaCa_2Mg_4AlSi_6Al_2O_{22}F_2$ is stable only under dry conditions and high *T* (1200 °C) and implies complete ordering of Al at the M2 site (Oberti et al. 1995a,b). In richterite, as well as in tremolite, OH is easily and completely exchanged by F during hydrothermal synthesis (Robert et al. 1999). However, despite the very similar local arrangement around the OH group, we observe here that in synthetic $Na(NaMg)Mg_5Si_8O_{22}(OH)_2$ there is no OH-F solid-solution under hydrous conditions, whereas synthetic $Na(NaMg)Mg_5Si_8O_{22}F_2$ can be obtained under dry conditions at high *T* (Gibbs et al. 1962; Raudsepp et al. 1991). This behavior is very unusual for an Al-free amphibole, and contradicts the findings of Robert et al. (2000) and Della Ventura et al. (2001). At present, we are unable to explain this behavior on the basis of structural or crystal-chemical control.

The crystal-structure of $Na(NaMg)Mg_5Si_8O_{22}(OH)_2$

Systematic extinctions and structure refinement show that the correct space group of synthetic $Na(NaMg)Mg_5Si_8O_{22}(OH)_2$ is $P2_1/m$, a subgroup of $C2/m$. The $P2_1/m$ amphibole structure has been previously described for low-T high-P Mg-rich cummingtonites (cf. Hawthorne 1983 for a discussion). With reference to cummingtonite, the samples of this work have two important features: the nearly complete occupancy of the A-group sites, and the presence of cations with very different ionic radii at the B-group sites (0.89 and 1.18 Å for Mg and Na in [8]-fold coordination, respectively; Shannon 1976). Structure refinement confirms that Na is equally partitioned between the A- and B-group sites according to the exchange vector $^A\square_1{}^BMg_1{}^ANa_{-1}{}^BNa_{-1}$, allowing electroneutrality of the structure. The two heterovalent substitutions must also couple locally to ensure constant bond-valence contributions to O5, O6, and O7. The only octahedral cation is Mg; the pattern of octahedral mean bond-lengths is M2-O > M1-O > M3-O, and is similar to what is found in other $^CMg_5(OH)_2$ $C2/m$ end-members such as tremolite and richterite.

At the B-group sub-sites, Mg has fivefold coordination (the M4 site), whereas Na has sevenfold coordination (the M4' site, shifted by ~ 0.3 Å from M4). The presence of cations with different ionic radii and coordination at the B-group sites, which connect the double-chains of tetrahedra with the octahedral strip, is particularly effective in allowing distinct geometrical configurations for the two independent chains of tetrahedra: the A chain tends to convert to S-rotation, whereas the B chain maintains the O rotation typical of the $C2/m$ structure. The kinking of the double chain along the **c** axis is usually expressed by the O5-O6-O5 angle. The measured O5-O6-O5 values for cummingtonite 1997-4 of Boffa Ballaran et al. (2000) annealed at 700 °C ($X_{Fe} = 0.34$ and $\langle^{[8]}r_{M4}\rangle = 0.91$ Å) are 183.6(1) and 161.6(1)° for the A and B double-chains, respectively. The two angles tend to converge for increasing $\langle^{[8]}r_{M4}\rangle$ in samples equilibrated at the same temperature. However, for sample 334 n. 2 ($X_{Fe} = 0$ and $\langle^{[8]}r_{M4}\rangle = 1.01$ Å) we obtained two very different values of 189.8(2)° and 158.6(2)°.

The kinking of the double chain along the **b** axis can be expressed by the T1-O7-T1 angle. Comparative analysis of the database available at CNR-IGG-PV for $C2/m$ amphiboles shows that this angle is inversely correlated with the mg no., and is positively correlated with both the size of the M4 polyhedron and the total A-site occupancy. Compared to cummingtonite, our amphibole has a larger M4 polyhedron and nearly complete A-site occupancy (both increase the T1-O7-T1 angle), as well as mg no. = 1 (which decreases the T1-O7-T1 angle). As the T1-O7-T1 values observed in crystal 334 n.2 (T1A-O7A-T1A = 139.1°; T1B-O7B-T1B = 135.3°) are smaller than in the most Mg-rich cummingtonite reported to date (T1A-O7A-T1A = 142.3°; T1B-O7B-T1B = 139.4°, sample 1997-4 ann. in Boffa-Ballaran et al. 2001), we conclude that the octahedral occupancy is the most important factor controlling the kinking of the double chain along the **b** direction.

The A cavity is bounded by two six-membered rings of tetrahedra belonging to two adjacent chains oriented base-to-base (Fig. 1). The A-cation position in samples with $P2_1/m$ symmetry is significantly off-set (~0.25 Å) along an imaginary line joining the two farthest O7A and O7B O atoms; in contrast to the $C2/m$ amphiboles, it does not repeat itself by symmetry within the A cavity. As a consequence, local order propagates along the chain solely by translation along [001]. Apart from this feature, the coordination of the cation at the A site in $P2_1/m$ amphiboles is analogous to that at the Am site in $C2/m$ amphiboles; however, it has two nearly equal A-O7A,B short distances (2.37 and 2.35 Å, respectively) and two different A-O7A,B long distances (3.62 and 3.92 Å, respectively).

Infrared spectroscopy

The infrared spectra collected in the OH-stretching region for the various experimental products are compared in Figure 4. The spectrum of sample 371 (synthesized at 750 °C) consists of two well-defined bands. The higher-frequency band, centered at 3742 cm^{-1}, is broader (FWHM = 30 cm^{-1}), and consists of at least three overlapping components, as suggested by shoulders on both sides of the main band. The lower-frequency band, centered at 3715 cm^{-1}, is sharper (FWHM = 20 cm^{-1}). This pattern is virtually identical to that published by Maresch and Langer (1976) and described by Raudsepp et al. (1991) for their nominal $Na(NaMg)Mg_5Si_8O_{22}(OH)_2$ amphiboles, which were actually both synthesized at 800 °C.

With increasing T of synthesis, a new band appears in the spectrum at 3667 cm^{-1} (Fig. 4). It is barely noticeable (3% out of total absorbance) in sample 403 (synthesized at 800 °C), but is prominent in samples 351 and 333 (synthesized at 850 and 900 °C, respectively); in the spectrum for the latter its intensity (height) is comparable to that of the 3715 cm^{-1} component.

Interpretation of the spectra

The spectra of Figure 4 can be interpreted with reference to the well-known spectrum of richterite (Fig. 5). The band at 3667

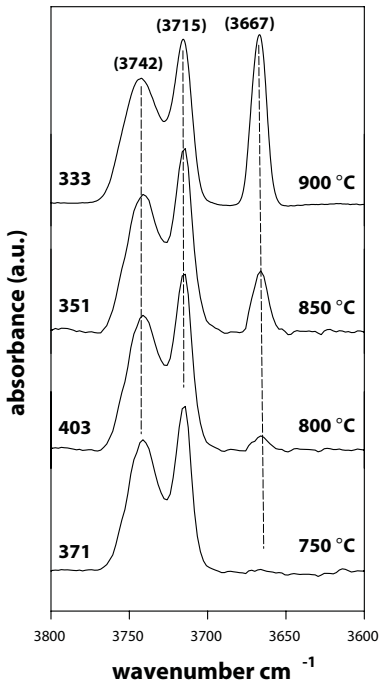

FIGURE 4. FTIR spectra in the OH-stretching region for nominal $Na(NaMg)Mg_5Si_8O_{22}(OH)_2$ at increasing T of synthesis.

cm^{-1} is assigned to OH directly bonded to three Mg octahedral cations, facing an empty A-site, i.e., to the MgMgMg-OH-$^{A}\square$ configuration (e.g., Maresch and Langer 1976; Rowbotham and Farmer 1973; Hawthorne et al. 1997). The frequency of this band is identical to that measured for cummingtonite (e.g., Boffa-Ballaran et al. 2001); the frequency shift with respect to the same absorption in richterite (3674 cm^{-1}) is due to an NNN effect of the different B-group site-populations (NaMg vs. NaCa; see also Iezzi et al. 2003). Therefore, the evolution of this band as a function of the *T* of synthesis is consistent with that of the unit-cell parameters and with the compositional variations.

Assignment of the main doublet in the 3700–3750 cm^{-1} region is less straightforward. Although it is present in the spectra published by Maresch and Langer (1976), no clear explanation has been given so far. On the basis of recent work on amphiboles of comparable composition, the higher-frequency component at 3742 cm^{-1} is assigned to OH directly bonded to three octahedral Mg cations, and facing an occupied A-site, i.e., to the MgMgMg-OH-^{A}Na configuration. Its frequency is close to that measured for richterite (e.g., Robert et al. 1989; Della Ventura 1992). Whereas richterite has *C*2/*m* symmetry (and thus one independent H atom), the samples of this work have $P2_1/m$ symmetry (and thus two independent H atoms). The position of the H atoms is difficult to determine with X-ray techniques, especially when the crystal is small and many reflections are very weak. Nevertheless, structural details obtained by SREF confirm that the environments of the two symmetry-independent H atoms are significantly different (Table 4). The 3742 cm^{-1} band is therefore assigned to the shorter O3B-H2 dipole, whereas the 3715 cm^{-1} band is assigned to the longer O3A-H1 dipole. This implies that IR spectroscopy can provide a fast and easy tool for the identification of non-equivalent OH-groups (i.e., of $P2_1/m$ symmetry) in the amphibole structure.

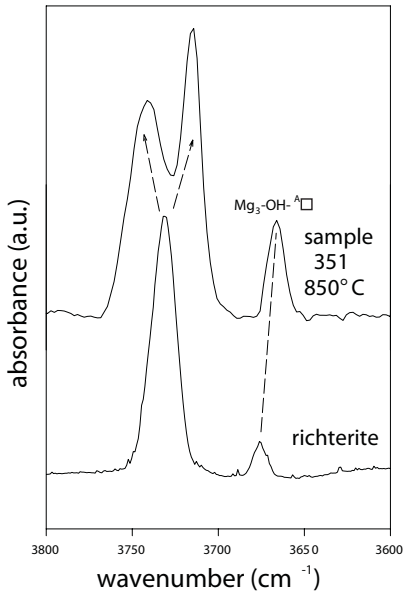

FIGURE 5. The FTIR spectrum of sample 351 compared to that of synthetic richterite (from Robert et al. 1989).

The stereochemistry around the A-cavity in $Na(NaMg)Mg_5Si_8O_{22}(OH)_2$

In amphiboles with occupied A sites, there is a strong repulsive interaction between H and the A cation, which is often alleviated by its off-centering onto the A*m* and A2 positions. This repulsion is consistent with the high frequency of the principal OH-band (Hawthorne et al. 1997). In synthetic $Na(NaMg)Mg_5Si_8O_{22}(OH)_2$, the broadness of the 3742 cm^{-1} band relative to the 3715 cm^{-1} band indicates that H2 interacts more strongly with ^{A}Na. A similar situation was observed by Robert et al. (1999) in richterites with mixed OH and F occupancy at the O3 site for which two main bands at 3730 and 3711 cm^{-1} related to the local OH-OH and OH-F environments, respectively, were observed. The broader shape of the 3730 cm^{-1} band was explained by a stronger interaction between H and ^{A}Na when the O3 site opposing across the cavity was occupied by OH.

In synthetic $Na(NaMg)Mg_5Si_8O_{22}(OH)_2$, the MgMgMg-OH-^{A}Na band splits into two components (i.e., shows a two-mode behavior; Chang and Mitra 1968) in response to the $C2/m \rightarrow P2_1/m$ change in symmetry (Fig. 5), whereas the MgMgMg-OH-$^{A}\square$ band is single (i.e., shows a one-mode behavior). This feature is consistent with the model for local coupling in the amphibole structure developed by Robert et al. (1999). In tremolite (as well as in cummingtonite), no coupling is possible between NNN O3 anions, either along the O3-O3 edge in the octahedral strip or across the vacant A-site cavity. As a consequence, OH groups facing empty A-sites are not coupled with adjacent but opposite OH groups facing occupied A-sites, and thus the MgMgMg-OH-$^{A}\square$ band is unique.

The band intensity in $Na(NaMg)Mg_5Si_8O_{22}(OH)_2$

Figure 6 shows the relation between the A-site occupancies derived from the integrated intensities of the 3667 cm^{-1} bands and those measured by EMPA. Previous work has shown that in tremolite-richterite solid-solutions, the molar fraction of tremolite (X_{tre}) can be derived from the relative intensity of the bands present in the IR spectrum when taking into account the difference in molar absorptivity between the two local A-site-vacant and A-site-occupied environments, which is $k = 2.16$ (Hawthorne

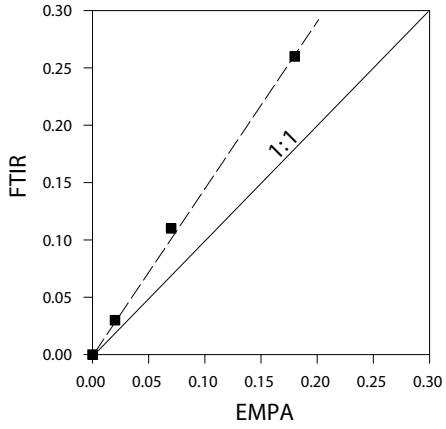

FIGURE 6. Comparison of the A-site vacancies derived from FTIR and the EMP analyses.

et al. 1997). Following Hawthorne et al. (1997), the value of k for the present system can be calculated by plotting $R/(1 - R)$ vs. $X_{cum}/(1 - X_{cum})$, where R is the relative intensity ratio between the A-site-vacant and the A-site-filled environments in synthetic $Na(NaMg)Mg_5Si_8O_{22}(OH)_2$ and X_{cum} is the molar fraction of A-vacant sites from EMPA (Table 6). The k value is the slope of the regression line ($R^2 = 0.99$), and is equal to 1.84 for the system investigated here. This value is reasonably similar to that given by Hawthorne et al. (1997) for an almost identical frequency range; however, the difference is significant, and suggests that other factors, such as local configurations, may affect the absorption coefficient. The good correlation in Figure 6 also corroborates the A-site populations derived from this work, and thus also the non-linear trends observed in Figure 3.

ACKNOWLEDGMENTS

The synthesis work described in this paper was done during the stay of G.I. at the Institut für Mineralogie of the Universität Hannover, for which financial support was provided by an EGIDE-Ministero degli Affari Esteri Italiano fellowship. H. Behrens and S. Ohlhorst kindly assisted during the experiments. Positive criticisms by D. Jenkins, F.C. Hawthorne, and M. Welch improved the final version of the manuscript.

REFERENCES CITED

Boffa Ballaran, T., Carpenter, M., and Domeneghetti, M.C. (2001) Phase transition and mixing behaviour of the cummingtonite-grunerite solid solution. Physics and Chemistry of Minerals, 28, 87–101.

Cámara, F., Oberti, R., Iezzi, G., and Della Ventura, G. (2003) The $P2_1/m \leftrightarrow C2/m$ phase transition in synthetic amphibole $Na\,NaMg\,Mg_5\,Si_8\,O_{22}\,(OH)_2$: Thermodynamic and crystal-chemical evaluation. Physics and Chemistry of Minerals, 30, 570–581.

Chang, I.F. and Mitra, S.S. (1968) Application of a modified random-element-isodisplacement model to long-wavelength optic phonons of mixed crystals. Physical Review, 172, 924–933.

Della Ventura, G. (1992) Recent developments in the synthesis and characterization of amphiboles. Synthesis and crystal-chemistry of richterites. Trends in Mineralogy, 1, 153–192.

Della Ventura, G., Robert, J.-L., Hawthorne, F.C., and Prost, R. (1996) Short-range disorder of Si and Ti in the tetrahedral double-chain unit of synthetic Ti-bearing potassium-richterite. American Mineralogist, 81, 56–60.

Della Ventura, G., Robert, J.-L. Sergent, J., Hawthorne, F.C., and Delbove, F. (2001) Constraints for the F-OH substitution in synthetic $^{[6]}$Al-bearing monoclinic amphiboles. European Journal of Mineralogy, 13, 841–847.

Downs, R.T. and Hall-Wallace, M. (2003) The American Mineralogist Crystal Structure Database. American Mineralogist, 88, 247–250.

Gibbs, G.V., Miller, J.L., and Shell, H.R. (1962) Synthetic fluor-magnesio-richterite. American Mineralogist, 47, 75–82.

Gier, T.E., Cox, N.L., and Young, H.S. (1964) The hydrothermal synthesis of sodium amphiboles. Inorganic Chemistry, 3, 1001–1004.

Hamilton, D.L. and Henderson, C.M.B. (1968) The preparation of silicate compositions by a gelling method. Mineralogical Magazine, 36, 832–838.

Hawthorne, F.C. (1983) The crystal chemistry of amphiboles. Canadian Mineralogist, 21, 173–480.

Hawthorne, F.C., Della Ventura, G., Robert, J.L, Welch, M.D., Raudsepp, M., and Jenkins, D.M. (1997) A Rietveld and infrared study of synthetic amphiboles along the potassium-richterite-tremolite join. American Mineralogist, 82, 708–716.

Iezzi, G., Della Ventura, G., Cámara, F., Pedrazzi, G., and Robert, J.L. (2003) $_B$Na–$_B$Li solid-solution A-site vacant amphiboles: synthesis and cation ordering along the ferri-clinoferroholmquistite—riebeckite join. American Mineralogist, 88, 955–961.

Jenkins, D.M. (1987) Synthesis and characterization of tremolite in the system H_2O–CaO–MgO–SiO_2. American Mineralogist, 72, 707–715.

Liu, S., Welch, M.D., Klinowski, J., and Maresch, W.V. (1996) A MAS NMR study of a monoclinic/triclinic phase transition in an amphibole with excess OH: $Na_3Mg_5Si_8O_{21}(OH)_3$ European Journal of Mineralogy, 8, 223–229.

Maresch, W.V and Langer, K. (1976) Synthesis, lattice constants and OH-valence vibrations of an orthorhombic amphibole with excess OH in the system Li_2O-MgO-SiO_2-H_2O. Contributions to Mineralogy and Petrology, 56, 27–34.

Maresch, W.V., Miehe, G., Czank, M., Fuess, H., and Schreyer, W. (1991) Triclinic amphibole. European Journal of Mineralogy, 3, 899–903.

Oberti, R., Hawthorne, F.C., Ungaretti, L., and Cannillo, E. (1995a) $^{[6]}$Al disorder in amphiboles from mantle peridotites. Canadian Mineralogist, 33, 867–878.

Oberti, R., Sardone, N., Hawthorne, F.C., Raudsepp, M., and Turnock, A.C. (1995b) Synthesis and crystal structure refinement of synthetic fluor-pargasite. Canadian Mineralogist., 33, 25–31.

Oberti, R., Ottolini, L., Della Ventura, G., and Prella, D. (2000) Excess OH in amphiboles: a structural model obtained by combining structure refinement, complete chemical characterization, and FTIR spectroscopy. Plinius, 24, 157.

Pouchou, J.L. and Pichoir, F. (1984) A new model for quantitative analysis: Part I. Application to the analysis of homogeneous samples. La Recherche Aerospatiale, 3, 13–38.

——— (1985) 'PAP' $\varnothing(\rho Z)$ procedure for improved quantitative micro-analysis. Microbeam Analysis, 104, 160.

Raudsepp, M., Turnock, A.C., and Hawthorne, F.C. (1991) Amphiboles synthesis at low pressure: what grows and what doesn't. European Journal of Mineralogy, 3, 983–1004.

Robert, J.L., Della Ventura, G., and Thauvin, J.-L. (1989) The infrared OH-stretching region of synthetic richterites in the system Na_2O-K_2O-CaO-MgO-SiO_2-H_2O-HF. European Journal of Mineralogy, 1, 203–211.

Robert, J.-L., Della Ventura, G., and Hawthorne, F.C. (1999) Near-infrared study of short-range disorder of OH and F in monoclinic amphiboles. American Mineralogist, 84, 86–91.

Robert, J.-L., Della Ventura, G., Welch, M., and Hawthorne, F.C. (2000) OH-F substitution in synthetic pargasite at 1.5 kbar, 850 °C. American Mineralogist, 85, 926–931.

Rowbotham, G. and Farmer, V.C. (1973) The effect of "A" site occupancy upon the hydroxyl stretching frequency in clinoamphiboles. Contributions to Mineralogy and Petrology, 38, 147–149.

Shannon, R.D. (1976) Revised effective ionic radii and systematic studies of interatomic distances in halides and chalcogenides. Acta Crystallographica, A32, 751–767.

Sheldrick, G.M. (1996) SADABS, Siemens area detector absorption correction software. University of Göttingen, Germany.

——— (1997) SHELXTL-97–A program for crystal structure refinement. University of Göttingen, Germany. Release 97-2.

Strens, R.G.J. (1974) The common chain, ribbon and ring silicates. In V.C. Farmer, Ed., The Infrared Spectra of Minerals. Mineralogical Society, Monographs, 4, 305–330. Mineralogical Society, London.

Wilke, M., Behrens, H., Burkhard, D.J.M., and Rossano, S. (2002) The oxidation state of iron in silicic melt at 500 MPa water pressure. Chemical Geology, 189, 55–67.

Wiles, D.B. and Young, P.A. (1981) A new computer program for Rietveld analysis of X-ray powder diffraction patterns. Journal of Applied Crystallography, 14, 149–151.

Witte, P., Langer, K., Seifert, F., and Schreyer, W. (1969) Synthetische amphibole mit OH-Überschuß im system Na_2O-MgO-SiO_2-H_2O. Naturwissenschaften, 56, 414–415.

Zimmerman, R., Heinrich, W., and Franz, G. (1996) Tremolite synthesis from $CaCl_2$-bearing acqueous solutions. European Journal of Mineralogy, 8, 767–776.

MANUSCRIPT RECEIVED APRIL 15, 2003
MANUSCRIPT ACCEPTED OCTOBER 19, 2003
MANUSCRIPT HANDLED BY PETER BURNS